Progress In Electromagnetics Research, Vol. 120, 459–479, 2011

ACTIVE LEARNING METHOD FOR THE DETERMINATION OF COUPLING FACTOR AND EXTERNAL Q IN MICROSTRIP FILTER DESIGN

P. Rezaee[1, 2, *], M. Tayarani[1], and R. Knöchel[2]

[1]Faculty of Electrical Engineering, Iran University of Science and Technology (IUST), Narmak, Tehran 16844, Iran

[2]Microwave Group, Christian-Albrechts-University of Kiel, Kiel 24143, Germany

Abstract—In the final step of any filter design process, the desired center frequency, coupling factor and external quality factor (Q_{ext}) are used to determine the physical parameters of the filter. Although in the most cases the physical dimensions of a single resonator for a given center frequency are determined using exact analytical or simple approximate equations, usually such simple equations cannot be found to easily relate the required coupling factor and Q_{ext} to the physical parameters of the filter. Analytical calculation of coupling factor and Q_{ext} versus dimensions are usually complicated due to the geometrical complexities or in some cases such as microstrip resonators due to the lack of exact solution for the field distribution. Therefore coupling factor and Q_{ext} of various kinds of resonators, especially microstrip resonators, are related to the physical parameters of the structure by the use of time consuming full wave simulations. In this paper a surprisingly fast and completely general approach based on a soft computing pattern-based processing technique, called active learning method (ALM) is proposed to overcome the time consuming process of coupling factor and Q_{ext} determination. At first the ALM technique and the steps of modeling are generally described, then as an example and in order to show the ability of the method this modeling approach is implemented to model the coupling factor and Q_{ext} surfaces of microstrip open-loop resonators versus physical parameters of the structure. Using the ALM-based extracted surfaces for coupling factor and Q_{ext}, two four pole Chebychev bandpass filters are designed and fabricated. Good agreement between the measured and simulated results validates the accuracy of the proposed approach.

Received 19 July 2011, Accepted 21 September 2011, Scheduled 30 September 2011

* Corresponding author: Payman Rezaee (pre@tf.uni-kiel.de).

1. INTRODUCTION

Modern communication systems need a complex arrangement of frequency allocation therefore a lot of different structures for the resonators and filters have been proposed to satisfy these requirements. In 1995 square open-loop resonators (SOLRs) were proposed by Hong [1]. They have been widely used in microwave filters due to their small size, planner structure and narrow realizable bandwidth. Although these resonators or other modified versions of them such as hexagonal [2–4] and spiral resonators [5, 6] have been used to realize canonical [7–13], dual [14–21], triple [22, 23] and quad-passband filters [24] with complicated transmission characteristics, all of these filters suffer from the time consuming full-wave-based process of determining the physical parameters of the filter from the desired coupling factor and Q_{ext}. The ability of soft computing techniques in modeling complicated problems in a vanishingly short time instead of using numerical or analytical approach [25–32] may provide a fast and accurate solution to this problem. Among the soft computing techniques the ability of fuzzy inference method in solving complicated electromagnetic problems such as microwave filter tuning [33, 34], EMC problems [35], resonant frequency computation [36, 37], determination of the transmission lines characteristic parameters [38], determination of the relative magnetic permeability [39] and also antenna modeling [40–42] has been proved in several publications. Artificial neural network (ANN) which is also a well-known soft computing technique has been used recently in microwave filter design [43]. Although the modeling steps of these methods seem to be very similar to the human logical thinking the amount and the complexity of the mathematics which is used, even in common fuzzy-based modeling techniques [44, 45], is usually forgotten. The time consuming process of ANN training and difficult interpretation of the knowledge embedded in the trained ANNs in a comprehensive form decreases the interest of using these modeling techniques if there is any alternative. ALM which is a relatively new soft computing technique does not suffer from the mathematical complexity of fuzzy algorithms and the difficult interpretability of ANN-based techniques [46, 47]. It has an intelligent information-handling process such as human brain and can be interpreted as a recursive fuzzy method which can express any multi-input single-output (MISO) system as the combination of some single-input single-output (SISO) one. Behavior of each SISO system which is a curve and a spread related to it will be extracted by the ink drop spread (IDS) method versus the corresponding independent variables. Then

using a proper combination rule of inference, the general behavior of the system is extracted.

Considering the simplicity, interpretability, fastness and accuracy of the ALM method, in this paper a completely general ALM-based approach for coupling factor and Q_{ext} computation is proposed. The paper is organized as follows. In the second section of the paper the concept of coupling factor and Q_{ext} is discussed briefly. The third and the fourth section of the paper are devoted to the basic definitions of ALM, clarifying the modeling steps using an illustrative example and its general formulation. In the fifth section the ALM technique is implemented to model the coupling factor and Q_{ext} of SOLRs versus three important physical parameters. Finally using the extracted coupling factor and Q_{ext} surfaces two four pole Chebychev bandpass filters are designed and fabricated. It should be mentioned that the modeling approach is completely general. It can be implemented to model coupling factor and Q_{ext} for each required physical parameter, other resonators or other feeding configurations. Considering more than three modeling parameters by the proposed approach is simply possible by adding its initial data to the former ones.

2. COUPLING STRUCTURES AND Q_{ext} DEFINITION

Shown in Figure 1 are three possible structures for the coupled SOLRs. The coupled structures result from different orientations of a pair of identical SOLRs which are separated by the spacing S. According to the nature of coupling which is through the fringe fields, three different types of coupling structures can be produced which are referred to as electric, magnetic and mixed coupling (Figure 1).

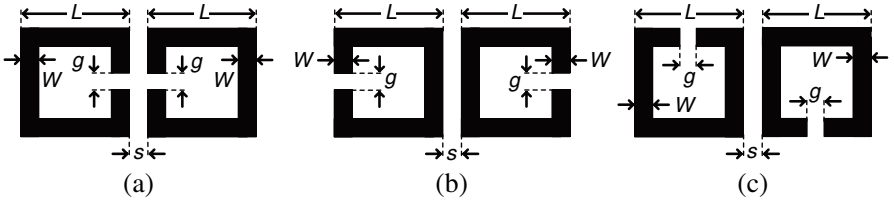

Figure 1. Coupled SOLRs in the case of, (a) electric coupling, (b) magnetic coupling, and (c) mixed coupling.

To calculate the coupling coefficient between two coupled resonators the following equation is used.

$$K = \frac{f_e^2 - f_m^2}{f_e^2 + f_m^2} \tag{1}$$

where f_e and f_m are the even and odd resonant frequencies of the two coupled resonators which occur in the frequencies that S_{11} has it's minimum value [7].

Another important step in the filter design process is the determination of Q_{ext} which is the coupling factor of a resonator to an external circuit. For every resonant circuit Q_{ext} can be computed by the aid of unloaded quality factor (Q_U) and loaded quality factor (Q_L) as it is shown in (2) [48].

$$\frac{1}{Q_{ext}} = \frac{1}{Q_L} - \frac{1}{Q_U} \tag{2}$$

Figure 2 shows a typical tapped-line feeding structure for a SOLR.

Using ALM method which will be described in the following sections the electric and magnetic coupling factor of SOLRs for three variables, i.e., the substrate permittivity (ε_r), the resonator length (L as shown in Figure 2) and the spacing between resonators (S) normalized to L (S_N which is equal to S/L) will be modeled in the range of [3 12], [6 mm 12 mm] and [0.08 0.35], respectively. Then Q_{ext} will be modeled versus the length (L_f), the width (W_f) and the position (D_f) of the feed line for two different tapped-line feeding structures which have been shown in Figures 2(a) and 2(b). The variation range of L_f, W_f and D_f are [5 mm 20 mm], [0.2 mm 1 mm], and [0 5 mm], respectively for the structure of Figure 2(a) and [5 mm 13 mm], [0.2 mm 1 mm], and [0 2 mm], respectively for the structure of Figure 2(b). Considering the modeled Q_{ext} surfaces provides a more efficient way in modeling this quantity. As it will be shown in the modeled surfaces, the variation of D_f itself can provide a wide variation range of Q_{ext} even when the L_f and W_f have been set to the fixed values. Considering this fact we have modeled Q_{ext} versus the resonator length, the substrate permittivity, and the normalized feed line position ($D_N = D_f^2/L$) in the variation range of [6 mm 12 mm], [3 12], and [0 0.6], respectively. Finally using these modeled Q_{ext} and coupling factor surfaces, one can design a SOLR filter

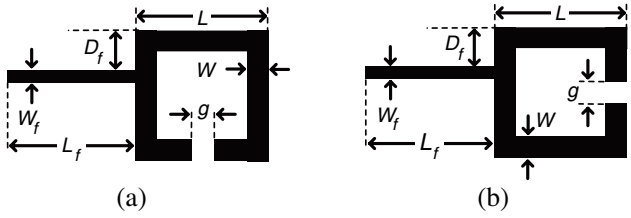

Figure 2. Typical tapped-line feeding structure for a SOLR.

within a relatively wide variation range of center frequency, fractional bandwidth and other required characteristics.

3. ALM DEFINITION

This section is devoted to the introduction of the ALM modeling technique, the major steps toward this modeling and its mathematical formulation which is accompanied by an illustrative example.

3.1. Major Steps of ALM Modeling

ALM uses the following steps to model an unknown system or function versus the total number of independent variables that affect its behavior or output value.

(i) At first, sample data is gathered by any numerical method or measurement technique.

(ii) In the second step which is usually called projection step, all the gathered data is projected on each x_i-y plane where x_i is the ith input variable and y stands for the output.
In this step we are trying to imagine that the system is composed of some SISO one. If the system was really a SISO one the projected data would provide a narrow unique path but because of the effect of other inputs a spread is detectable around each narrow path. This spread shows the effect of other input variables on the corresponding x_i-y plane. It can be easily deduced that, the narrower this spread, the effects of other input parameters on the output computation are less.

(iii) In the third step the narrow path and its related spread for each x_i-y plane is extracted by a method called ink drop spread (IDS) algorithm. This algorithm will be thoroughly discussed in the following sub-section.

(iv) Then appropriate fuzzy rules of inference are implemented to combine all the extracted narrow paths and spreads.

(v) Finally the calculated output is compared with the original output by a predefined threshold error.

(vi) If the model is not accurate enough, the input domains will be divided in more sections and if it is necessary intermediate data points will be added to the previous ones. The active learning method is run again to reduce the error of the model.

In the next sub-section the mathematical formulation of the method will be described. The modeling steps will also be clarified by an example.

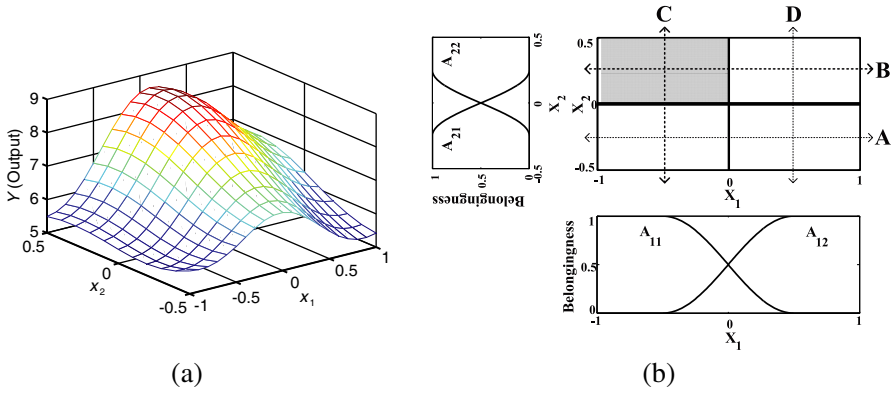

(a) (b)

Figure 3. (a) Input-output relationship of a system, and (b) input domains division and corresponding membership functions.

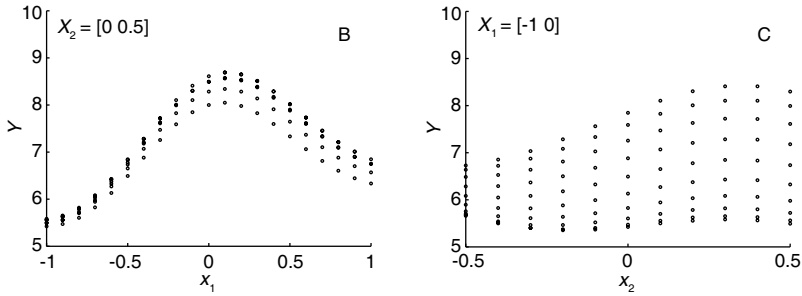

Figure 4. Projected data on the corresponding x_i-y plane for the parts B and C.

3.2. Illustrative Example and Mathematical Formulation

In order to explain the modeling process of ALM, we use a two-input function that has an input-output relationship as shown in Figure 3(a). For the simplicity of explanation each input domain is divided into two parts as shown in Figure 3(b), therefore four SISO systems are generated, i.e., A, B, C and D. In this figure A_{ij} is the jth membership function for the ith input variable. Projected data of parts B and C on the corresponding x_i-y plane are shown in Figure 4.

In order to extract the behavior of the system in the shaded area of Figure 3(b) which is in fact the intersection of SISO systems, B and C, it is only necessary to consider x_1 in the interval $[-1\ 0]$ of the part B and x_2 in the interval $[0\ 0.5]$ of the part C. As it can be seen in Figure 4, for the mentioned interval of x_2 in the part C a wide spread

is detectable, therefore no information about the output can be elicited from this projected data. On the other hand, in the mentioned interval for the x_1 in the part B there is a thin spread which means a high correlation between x_1 and the output. Therefore part B effectively elicits the system feature of the shaded area. In order to extract the behavior of the system in the total variation range of the inputs all data of parts A to D should be utilized. For each of these parts the related narrow path which explains the behavior of the corresponding SISO system and the related spread which explains the effect of other inputs on the extracted narrow path are obtained using IDS algorithm. Therefore following paragraphs are devoted to the explanation of the IDS method.

In the IDS method we assume each data point in each x_i-y plane as a light source which has a cone shape beamwidth. When the vertical distance from this point increases its pattern spreads and interferes with the pattern of other data points which are now other sources of light. Indeed these cones are three dimensional membership functions which show the degree of confidence to other points near data points. If the mixed patterns are plotted on the corresponding input-output plane in grayscale as shown in Figure 5, a narrow path can be extracted using (3). The process of grayscale representation of the data in each x_i-y plane is called IDS.

$$\begin{aligned} \psi(x_p) = &\left\{ (k\Delta y + y_{\min}) \left| \sum\nolimits_{q=0}^{k} d(x_p, y_q) \approx \sum\nolimits_{q=k+1}^{N} d(x_p, y_q) \right. \right\} \\ &x_p = x_{\min} + p\Delta x;\ y_q = y_{\min} + q\Delta y;\ x = [x_{\min}, x_{\min} + M\Delta x] \\ &y = [y_{\min}, y_{\min} + N\Delta y];\ p = 0, 1, \ldots, M;\ q = 0, 1, \ldots, N; \\ &0 < k < N \end{aligned} \quad (3)$$

where $\psi(x)$ is the extracted narrow path for the input parameter x. $d(a, b)$ is the value of darkness in point (a, b). This value is 1 for the darkest points which are the most confident points in the plane and is 0 for the lightest ones. To compute the spread for each value of input

Figure 5. A typical IDS pattern.

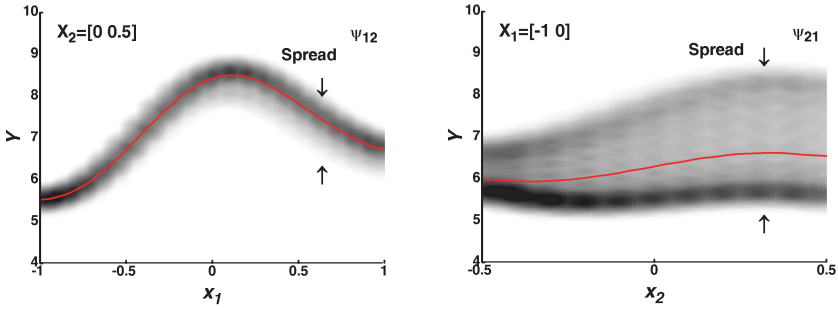

Figure 6. Extracted narrow paths and IDS patterns of Figure 4.

the width of the dark area in y direction is calculated using (4).

$$\sigma(x) = \max\{y|d(x,y) > 0\} - \min\{y|d(x,y) > 0\} \tag{4}$$

In Figure 6 the IDS pattern and the narrow path for each of the SISO systems in Figure 4 has been extracted using the mentioned approach. Spreads can be extracted using (4). All the extracted narrow paths and spreads are used in the inference process. In the above example each input domain was divided into two sections therefore we have only four inference rules as follows:

$$\begin{aligned} &R_{11}\text{: If } x_2 \text{ is } A_{21}, \text{ then } y \text{ is } \psi_{11} \\ &R_{12}\text{: If } x_2 \text{ is } A_{22}, \text{ then } y \text{ is } \psi_{12} \\ &R_{21}\text{: If } x_1 \text{ is } A_{11}, \text{ then } y \text{ is } \psi_{21} \\ &R_{22}\text{: If } x_1 \text{ is } A_{12}, \text{ then } y \text{ is } \psi_{22} \end{aligned} \tag{5}$$

where ψ_{ij} is the jth narrow path for the ith input variable and A_{ij} denotes the jth membership function for the ith input variable. Assuming x as variable, the general form of the membership functions can be expressed as follows:

$$\begin{cases} 0.5 \times (1 + \cos\pi((x-a)/(b-a))) & \text{for} \quad x{:}a \to b \\ 0.5 \times (1 - \cos\pi((x-a)/(b-a))) & \text{for} \quad x{:}a \to b \end{cases} \tag{6}$$

Finally the model output is obtained by aggregating the narrow paths as follows:

$$y \text{ is } \beta_{11}\psi_{11} \text{ or } \beta_{12}\psi_{12} \text{ or } \beta_{21}\psi_{21} \text{ or } \beta_{22}\psi_{22} \tag{7}$$

where y is the output of the model, or is the union operator and β_{ij} denotes the weight of jth narrow path for the ith input variable. The

value of β is determined from the spread and the degree of truth of the antecedent part in (5). It can be calculated as follows:

$$\begin{aligned}\beta_{1k_1} &= (\omega_{1k_1} \times A_{2k_1})/(\omega_{11} \times A_{21} + \omega_{12} \times A_{22} \\ &\quad + \omega_{21} \times A_{11} + \omega_{22} \times A_{12}) \\ \beta_{2k_2} &= (\omega_{2k_2} \times A_{1k_2})/(\omega_{11} \times A_{21} + \omega_{12} \times A_{22} \\ &\quad + \omega_{21} \times A_{11} + \omega_{22} \times A_{12}) \\ \omega_{ij} &= 1/\sigma_{ij};\ i = 1, 2;\ j = 1, 2;\ k_1 = 1, 2;\ k_2 = 1, 2\end{aligned} \tag{8}$$

4. ALM FOR THREE-INPUT SYSTEMS

In this section the ALM formulation for modeling of an unknown function with three independent variables which are referred to as x_1, x_2 and x_3 is described. After gathering input-output data in the range of independent variables each input domain is divided into m_1, m_2 and m_3 partitions, respectively. In the next step the gathered data are projected on the corresponding x_i-y plane for IDS processing which means the extraction of narrow path and spread for each SISO system. The number of IDS units is calculated as follows:

$$L = \sum\nolimits_{i=1}^{3} l_i \quad l_i = \prod\nolimits_{\substack{j=1 \\ j \neq i}}^{3} m_j \tag{9}$$

where L is the total number of all IDS units and l_i denotes the number of IDS units for the input variable x_i.

All the extracted narrow paths and spreads are utilized in the inference process. The number of inference rules is equal to L. Some of these inference rules are shown in (10).

$$\begin{aligned}&R_{11}\text{: If } x_2 \text{ is } A_{21} \text{ and } x_3 \text{ is } A_{31} \text{ then } y \text{ is } \psi_{11} \\ &\vdots \\ &R_{1l_1}\text{: If } x_2 \text{ is } A_{2m_2} \text{ and } x_3 \text{ is } A_{3m_3} \text{ then } y \text{ is } \psi_{1l_1} \\ &R_{21}\text{: If } x_1 \text{ is } A_{11} \text{ and } x_3 \text{ is } A_{31} \text{ then } y \text{ is } \psi_{21} \\ &\vdots \\ &R_{3l_3}\text{: If } x_1 \text{ is } A_{1m_1} \text{ and } x_2 \text{ is } A_{2m_2} \text{ then } y \text{ is } \psi_{3l_3}\end{aligned} \tag{10}$$

Finally the output of the system is calculated by aggregating the narrow paths using (11).

$$\begin{aligned}&y \text{ is } \beta_{11}\psi_{11} \text{ or } \ldots \text{ or } \beta_{ik}\psi_{ik} \text{ or } \ldots \text{ or } \beta_{3l_3}\psi_{3l_3} \\ &k = 1, 2, \ldots, l_i;\quad i = 1, 2, 3\end{aligned} \tag{11}$$

where β_{ik} is calculated as follows:

$$\beta_{ik} = \frac{\omega_{ik} \times \Gamma_{ik}}{\sum_{i=1}^{3} \sum_{k=1}^{l_i} \omega_{ik} \times \Gamma_{ik}} \tag{12}$$

In this equation Γ_{ik} is calculated using (13).

$$\begin{aligned} \Gamma_{11} &= A_{21} \wedge A_{31}, \ldots, \Gamma_{1l_1} = A_{2m_2} \wedge A_{3m_3} \\ \Gamma_{21} &= A_{11} \wedge A_{31}, \ldots, \Gamma_{2l_2} = A_{1m_1} \wedge A_{3m_3} \\ \Gamma_{31} &= A_{11} \wedge A_{21}, \ldots, \Gamma_{3l_3} = A_{1m_1} \wedge A_{2m_2} \end{aligned} \tag{13}$$

where $\wedge$ is the intersection operator of the fuzzy sets.

5. COUPLING AND Q_{ext} MODELING

In this section the effect of substrate permittivity, resonator length and spacing between resonators on the electric and magnetic coupling factor will be modeled using the discussed modeling technique. Then for the structures shown in the Figure 2 the effect of feed line length, feed line position and feed line width on the Q_{ext} will be modeled. For all of these modeling the height of the substrate (h), the width of the resonator (W) and the gap size (g) are selected to be equal to 1.27 mm, 1 mm, and 1 mm, respectively. In the Q_{ext} modeling, for the structure of Figures 2(a) and 2(b), L is selected equal to 10.5 mm, and 6.5 mm, respectively. Parameters variation range have been mentioned in the last paragraph of the Section 2.

The following steps have been carried out to construct the ALM-based coupling factor and Q_{ext} surfaces:

(i) Electric and magnetic coupling factors have been calculated using Ansoft HFSS-13 for 176 points within the variation range of the modeling parameters, i.e., L, ε_r and S_N. These are the input data of our model for coupling factor computation. In the same way, Q_{ext} of Figures 2(a) and 2(b) has been calculated using Ansoft HFSS-13 for 140 and 120 data points, respectively within the variation range of W_f, L_f and D_f. These calculations provide the input data of our model for Q_{ext} computation.

(ii) Concerning the electric and magnetic coupling factor modeling, the variation range of L, ε_r and S_N has been divided into 3, 3, and 10 sections, respectively. Concerning the Q_{ext} modeling, the variation range of W_f, L_f and D_f has been divided into 4, 3, and 6 sections, respectively for the structure of Figure 2(a) and 5, 3, and 4 sections, respectively for the structure of Figure 2(b).

(iii) The narrow path and spread of each of these divisions has been computed by (3) and (4), respectively.

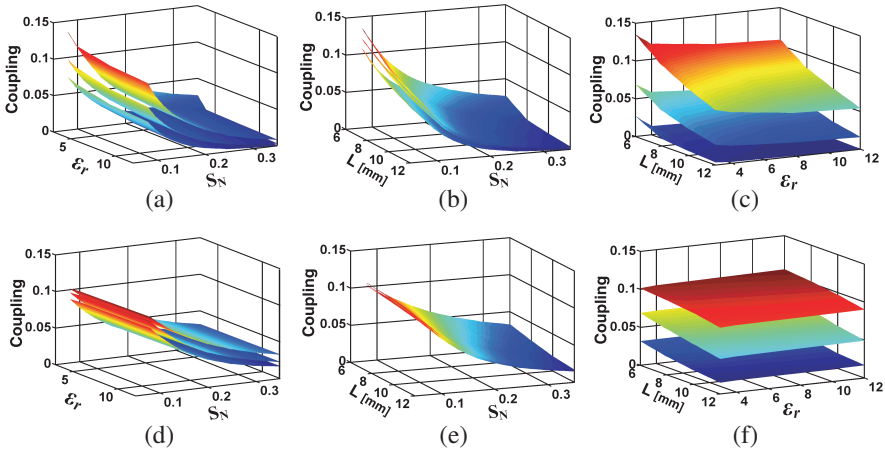

Figure 7. Extracted electric coupling surfaces; (a) $L = 6\,\text{mm}$ (top), $L = 9\,\text{mm}$ (middle), $L = 12\,\text{mm}$ (bottom), (b) $\varepsilon_r = 3$ (top), $\varepsilon_r = 4$ (middle), $\varepsilon_r = 12$ (bottom), and (c) $S_N = 0.08$ (top), $S_N = 0.16$ (middle), $S_N = 0.35$ (bottom). Extracted magnetic coupling surfaces; (d) $L = 6\,\text{mm}$ (top), $L = 9\,\text{mm}$ (middle), $L = 12\,\text{mm}$ (bottom), (e) $\varepsilon_r = 12$ (top), $\varepsilon_r = 4$ (middle), $\varepsilon_r = 3$ (bottom), and (f) $S_N = 0.08$ (top), $S_N = 0.16$ (middle), $S_N = 0.35$ (bottom).

(iv) Using the inference rules (10), the computed narrow paths, and spreads the output has been calculated by (11).

Each of the extracted ALM-based surfaces, i.e., electric and magnetic coupling factor surfaces and the Q_{ext} surfaces, has three variables. Therefore it is not possible to show each of them in one figure. Figures 7 and 8 show the extracted surfaces versus two of the modeling parameters. In each of these figures one of the independent variables has been set to three different values and the other ones sweep their own range of variations.

Considering Figures 7(a)–7(c) it can be deduced that the electric coupling factor is mainly influenced by the normalized spacing, mildly influenced by the resonator length, and weakly influenced by the substrate permittivity. In the same way, considering Figures 7(d)–7(f) it can be seen that the magnetic coupling is also mainly influenced by the normalized spacing, mildly influenced by the resonator length, but very weakly influenced by the substrate permittivity.

Figures 8(a)–8(c) illustrate the fact that the Q_{ext} for the structure which has been shown in Figure 2(a) is equally influenced by the length, the width, and the position of the feed line. Q_{ext} of the

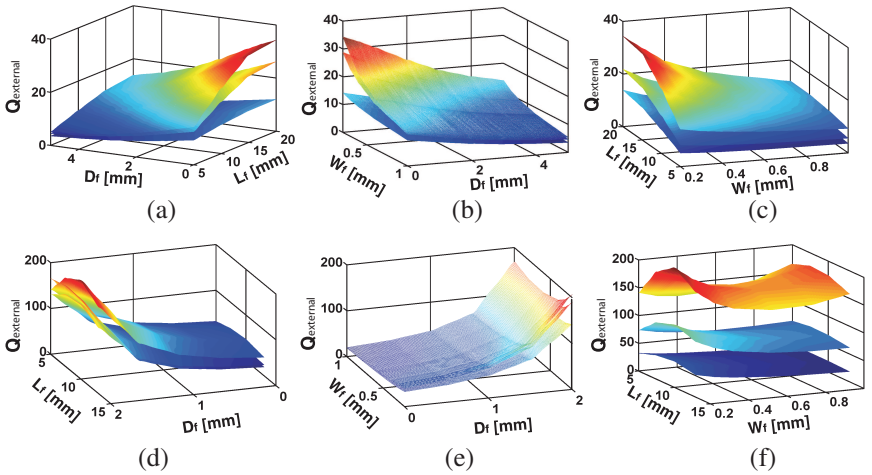

Figure 8. Extracted Q_{ext} for the structure of Figure 2(a); (a) $W_f = 0.2\,\text{mm}$ (top), $W_f = 0.35\,\text{mm}$ (middle), $W_f = 1\,\text{mm}$ (bottom), (b) $L_f = 20\,\text{mm}$ (top), $L_f = 12.5\,\text{mm}$ (middle), $L_f = 5\,\text{mm}$ (bottom), and (c) $D_f = 0$ (top), $D_f = 2.5\,\text{mm}$ (middle), $D_f = 5\,\text{mm}$ (bottom). Extracted Q_{ext} for the structure of Figure (2b); (d) $W_f = 0.2\,\text{mm}$ (top), $W_f = 1\,\text{mm}$ (middle), $W_f = 0.6\,\text{mm}$ (bottom), (e) $L_f = 11\,\text{mm}$ (top), $L_f = 13\,\text{mm}$ (middle), $L_f = 5\,\text{mm}$ (bottom), and (f) $D_f = 2\,\text{mm}$ (top), $D_f = 1.5\,\text{mm}$ (middle), $D_f = 0$ (bottom).

Figure 2(b) is shown in Figures 8(d)–8(f). These figures show that the Q_{ext} drastically influenced by the feed line position while the influence of the feed line width and length is much weaker. Figures 8(a)–8(f) also illustrate that the feeding structure of Figure 2(a) can not be used to design very narrow band filters due to the fact that this structure can not provide high values of Q_{ext}.

Considering the Q_{ext} surfaces depicted in Figures 8(a)–8(f) provides a more efficient way in modeling this quantity. As it can be concluded from these figures variation of the feed line position (D_f) itself can provide a wide variation range of Q_{ext} even when the feed line length and feed line width have been set to the appropriate fixed values. Considering this fact and the capability of the structure shown in Figure 2(b) in providing different values of Q_{ext}, we have modeled the Q_{ext} of Figure 2(b) versus the resonator length, the substrate permittivity, and the normalized feed line position (D_N). These modeled Q_{ext} and coupling factors provide the required tool for designing SOLR filters in a wide variation range of electrical

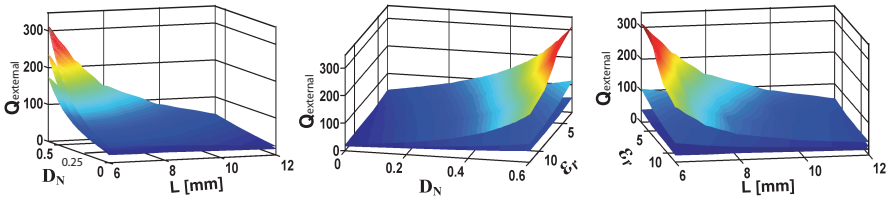

Figure 9. Extracted Q_{ext} for the structure of Figure 2(b) for the new modeling parameters; (a) $\varepsilon_r = 3$ (top), $\varepsilon_r = 7.5$ (middle), $\varepsilon_r = 12$ (bottom), (b) $L = 6\,\text{mm}$ (top), $L = 9\,\text{mm}$ (middle), $L = 12\,\text{mm}$ (bottom), and (c) $D_N = 0.6$ (top), $D_N = 0.3$ (middle), $D_N = 0$ (bottom).

characteristics such as center frequency and fractional bandwidth. In this modeling process, L_f, W_f, W, g, and h have been selected equal to 10 mm, 0.8 mm, 1 mm, 1 mm, and 1.27 mm, respectively. Modeling process is similar to the procedure which has been mentioned before. Figure 9 shows the sample results of the extracted data.

These Q_{ext} and coupling factor surfaces not only provide a powerful design tool for SOLR filters but also provide the possibility of estimating the sensitivity of the electrical characteristics of the filter to each one of the modeling parameters. In other words the effect of fabrication or the substrate permittivity tolerances can be easily taken into account using these surfaces.

It should be mentioned that the coupling factor and Q_{ext} surfaces have been extracted within the total variation range of the three modeling parameters. Resolution of the extracted data is equal to 0.01 mm for L, W_f, L_f, and D_f, 0.01 for ε_r, and is equal to 0.001 for S_N and D_N. Considering the above mentioned resolution each of the magnetic or electric coupling surfaces consists of $601 \times 901 \times 271$ points. ALM needs less than half an hour for modeling each of these electric or magnetic coupling surfaces while Ansoft HFSS-13 needs 3 minutes for each point of these coupling surfaces. In other words, Ansoft HFSS-13 needs about 837 years for computing each of these surfaces.

In order to verify the model accuracy, the error between the target function (full-wave-based extracted data) and the constructed model (ALM-based extracted data) was measured using two different criteria, i.e., the fraction of variance unexplained (FVU) and correlation

coefficient (CC) which are defined as follows.

$$\mathrm{FVU} = \frac{\sum_{l=1}^{N} (y_l - \hat{y}_l)}{\sum_{l=1}^{N} \left(y_l - \bar{A}\right)^2} \tag{14}$$

$$\mathrm{CC} = \frac{\sum_{l=1}^{N} \left(y_l - \bar{A}\right)\left(\hat{y}_l - \bar{B}\right)}{\sqrt{\left(\sum_{l=1}^{N} \left(y_l - \bar{A}\right)^2\right)\left(\sum_{l=1}^{N} \left(\hat{y}_l - \bar{B}\right)^2\right)}} \tag{15}$$

where y_l and $\hat{y}_l$ denotes the lth data point of the output vector and the constructed model, respectively. $\bar{A} = \frac{1}{N}\sum_{l=1}^{N} y_l$, $\bar{B} = \frac{1}{N}\sum_{l=1}^{N} \hat{y}_l$, and N is the total number of output vector.

FVU is proportional to the mean square error. As the model accuracy increases, the FVU approaches zero and CC approaches one. Shown in Figure 10 are three coupling curves result from setting the substrate permittivity equal to 9.8 and the resonator length equal to the three different fixed values (6.5, 8.5, and 10.5 mm) in the extracted three-input ALM-based electric and magnetic coupling factors. Full-wave-based simulation results which have been calculated using Ansoft HFSS-13 are also included in these figures for the comparison purpose. As it is seen they are in good agreement. FVU and CC calculation results validate again the accuracy of the extracted surfaces quantitatively. FVU is equal to 0.0002, 0.0007, and 0.0003 for the Figures 10(a), 10(b), and 10(c), respectively, and CC is equal to 0.9999 for all of these figures.

The above mentioned results clearly show the ability of ALM technique in providing a completely fast, accurate and general modeling tool for coupling factor and Q_{ext} computation within a

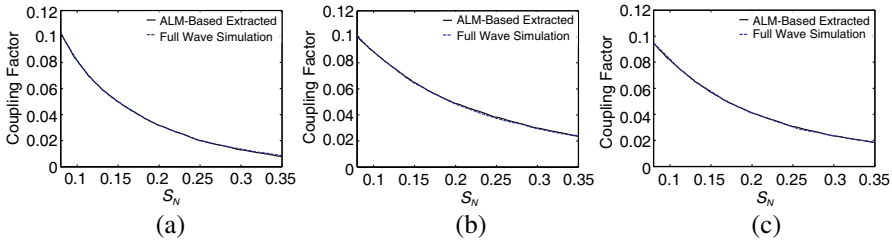

Figure 10. Coupling factor curves result from setting substrate permittivity equal to 9.8 and the resonator length (L) equal to the three different values in the extracted three-input ALM-based electric and magnetic coupling factors accompany with the full wave simulation results, (a) $L = 6.5$ mm (electric coupling), (b) $L = 8.5$ mm (magnetic coupling), and (c) $L = 10.5$ mm (magnetic coupling).

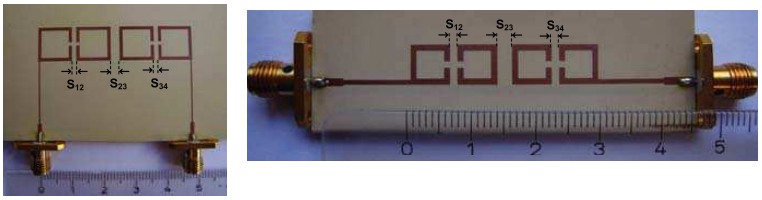

(a) (b)

Figure 11. Fabricated filters, (a) filter 1, and (b) filter 2.

wide variation range of the physical parameters. Providing such a design tool using full wave simulators is almost impossible due to the tremendous amount of simulation time.

6. FILTER DESIGN USING EXTRACTED SURFACES

To show the accuracy of the extracted coupling factor and Q_{ext} surfaces, two four pole Chebychev bandpass filters were designed with the fractional bandwidth of 4% and the center frequencies of 1.64 GHz and 2.95 GHz which are referred to as filter 1 and filter 2, respectively. Figures 11(a) and 11(b) show the physical structure of the fabricated filters.

For the above mentioned fractional bandwidth Q_{ext} is equal to 24 and the coupling matrix is given by 16.

$$\begin{bmatrix} 0 & 0.0359 & 0 & 0 \\ 0.0359 & 0 & 0.0277 & 0 \\ 0 & 0.0277 & 0 & 0.0359 \\ 0 & 0 & 0.0359 & 0 \end{bmatrix} \tag{16}$$

Both of the filters were fabricated on a Rogers substrate (TMM10i) with a relative permittivity of 9.8 and thickness of 1.27 mm. As it was mentioned before the resonator gap and width both were selected to be 1 mm. To satisfy required center frequencies, L (Figure 2) was selected equal to 10.5 mm and 6.5 mm for the filters 1 and 2, respectively. Considering the physical structure of the filters 1 and 2 (Figure 11) it can be easily deduced that for both of the filters the first and the last two resonators are electrically coupled while the second and the third resonators are magnetically coupled. Therefore the spacing between the electrically coupled resonators, i.e., S_{12} and S_{34} (Figure 11) can be determined easily using extracted electric coupling factor surfaces. Considering the ($L = 10.5$ mm, $\varepsilon_r = 9.8$) cut of these surfaces for the first filter and ($L = 6.5$ mm, $\varepsilon_r = 9.8$) cut of them for the second filter will result in two curves which determines the electrical coupling values

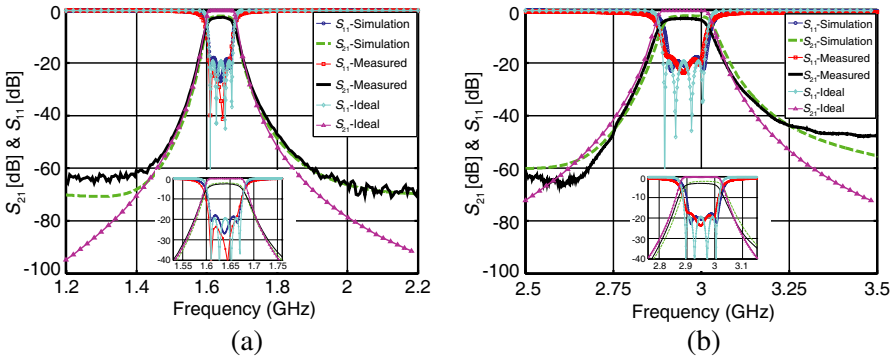

Figure 12. Responses of the filters, (a) filter 1, and (b) filter 2.

for both of the filters versus spacing between resonators. These curves result in $S_{12} = S_{34} = 1.3\,\text{mm}$ for the filter 1 and $S_{12} = S_{34} = 1.2\,\text{mm}$ for the filter 2. In the same way, the spacing between magnetically coupled resonators, i.e., S_{23} can be determined easily using extracted magnetic coupling factor surfaces and the resulted magnetic coupling curves for each of the filters. These curves result in $S_{23} = 2.7\,\text{mm}$ for the filter 1 and $S_{23} = 2.4\,\text{mm}$ for the filter 2. Using ALM-based extracted Q_{ext} surfaces, for $Q_{ext} = 24$ various triplets of (L_f, W_f, D_f) were calculated. Among these different choices, L_f, W_f and D_f were selected 19 mm, 0.4 mm, and 0.2 mm, respectively for the filter 1 and 11.25 mm, 0.8 mm, and 0, respectively for the filter 2.

The simulated, the measured, and the ideal responses of the filters are shown in Figure 12. As it is seen they are in good agreement which shows the accuracy of the ALM-based extracted coupling factor and Q_{ext} surfaces.

7. CONCLUSIONS

A novel approach based on ALM has been proposed to model coupling factor and Q_{ext} of SOLRs. This ALM-based modeling approach has been implemented to model the coupling factor of electrically and magnetically coupled SOLRs versus three important effective parameters, i.e., spacing between resonators, resonator length and substrate permittivity. Using the same approach Q_{ext} of a SOLR has been modeled versus important parameters which are feed line length, feed line width and feed line position. Afterwards Q_{ext} was modeled versus a new set of modeling parameters, i.e., the position of the feed line, the length of the resonator and the permittivity of the

substrate. Based on the extracted coupling factor and Q_{ext} surfaces two filters were designed and fabricated. Good agreement between the measured responses of the filters and the simulated ones validates the accuracy of the extracted surfaces. Although the model is very simple in its structure it is surprisingly fast and as accurate as the other time consuming and complicated numerical methods. The modeling approach is general and can be used for other kinds of coupling, other resonators or other feeding structures with the same degree of simplicity. It is also possible to consider more than three parameters in the proposed modeling approach easily if we add initial required data of the new parameters to the previous ones. This surprisingly fast method provides the possibility of modeling unknown functions within a wide variation range of modeling parameters with a high resolution of the extracted data. This resolution is not accessible through the use of full wave simulators due to the tremendous amount of simulation time.

REFERENCES

1. Hong, J. S. and M. J. Lancaster, "Canonical microstrip filter using square open-loop resonators," *IEE Electron. Lett.*, Vol. 31, No. 23, 2020–2022, Nov. 1995.
2. Mao, R. J., X. H. Tang, L. Wang, and G. H. Du, "Miniaturized hexagonal stepped-impedance resonators and their applications to filters," *IEEE Trans. Microwave Theory Tech.*, Vol. 56, No. 2, 440–448, Feb. 2008.
3. Mo, S.-G., Z.-Y. Yu, and L. Zhang, "Compact dual-mode bandpass filters using hexagonal meander loop resonators," *Journal of Electromagnetic Waves and Applications*, Vol. 23, No. 13, 1723–1732, 2009.
4. Mo, S.-G., Z.-Y. Yu, and L. Zhang, "Design of triple-mode bandpass filter using improved hexagonal loop resonator," *Progress In Electromagnetics Research*, Vol. 96, 117–125, 2009.
5. Dai, G.-L. and M.-Y. Xia, "An investigation of quarter-wavelength square-spiral resonator and its applications to miniaturized bandpass filters," *Journal of Electromagnetic Waves and Applications*, Vol. 24, No. 10, 1303–1313, 2010.
6. Alhawari, A. R. H., A. Ismail, M. F. A. Rasid, R. S. A. R. Abdullah, B. K. Esfeh, and H. Adam, "Compact microstrip bandpass filter with sharp passband skirts using square spiral resonators and embedded-resonators," *Journal of Electromagnetic Waves and Applications*, Vol. 23, No. 5–6, 675–683, 2009.

7. Hong, J. S. and M. J. Lancaster, "Coupling of microstrip square open-loop resonators for cross-coupled planar microwave filters," *IEEE Trans. Microwave Theory Tech.*, Vol. 44, No. 12, 2099–2109, Dec. 1996.
8. Hong, J. S., M. J. Lancaster, R. B. Greed, and D. Jedamzik, "On the development of superconducting microstrip filters for mobile communications applications," *IEEE Trans. Microwave Theory Tech.*, Vol. 47, No. 9, 1656–1663, Sep. 1999.
9. Fan, J.-W., C.-H. Liang, and X.-W. Dai, "Design of cross-coupled dual-band filter with equal-length split-ring resonators," *Progress In Electromagnetics Research*, Vol. 75, 285–293, 2007.
10. Wen, S. and L. Zhu, "Numerical synthesis design of coupled resonator filters," *Progress In Electromagnetics Research*, Vol. 92, 333–346, 2009.
11. Weng, M. H., C. H. Kao, and Y. C. Chang, "A compact dual-band bandpass filter with high band selectivity using cross-coupled asymmetric SIRs for WLANs," *Journal of Electromagnetic Waves and Applications*, Vol. 24, Nos. 2–3, 161–168, 2010.
12. Jiang, S. M., W.-T. Li, X. H. Wang, Q. Y. Song, and X.-W. Shi, "A novel method of designing cross-coupled filters through optimization," *Journal of Electromagnetic Waves and Applications*, Vol. 23, No. 14–15, 2011–2019, 2009.
13. Zhu, Y.-Z., H. S. Song, and K. Guan, "Design of optimized selective quasi-elliptic filters," *Journal of Electromagnetic Waves and Applications*, Vol. 23, No. 10, 1357–1366, 2009.
14. Lee, J. and K. Sarabandi, "A synthesis method for dual-passband microwave filters," *IEEE Trans. Microwave Theory Tech.*, Vol. 55, No. 6, 1163–1170, Jun. 2007.
15. Athukorala, L., D. Budimir, and M. M. Potrebic, "Design of open-loop dual-mode microstrip filters," *Progress In Electromagnetics Research Letters*, Vol. 19, 179–185, 2010.
16. Lin, H.-J., X.-Q. Chen, X.-W. Shi, L. Chen, and C.-L. Li, "A dual passband filter using hybrid microstrip open loop resonators and coplanar waveguide slotline resonators," *Journal of Electromagnetic Waves and Applications*, Vol. 24, No. 1, 141–149, 2010.
17. Rebenaque, D. C., J. Pascual-García, F. Q. Pereira, J. L. Gomez-Tornero, and A. A. Melcon, "Novel implementation of transversal filters in multilayered microstrip technology," *Journal of Electromagnetic Waves and Applications*, Vol. 24, No. 8–9, 1241–1253, 2010.

18. Abu-Hudrouss, A. M. and M. J. Lancaster, "Design of multiple-band microwave filters using cascaded filter elements," *Journal of Electromagnetic Waves and Applications*, Vol. 23, No. 16, 2109–2118, 2009.
19. Lai, X., N. Wang, B. Wu, and C.-H. Liang, "Design of dual-band filter based on OLRR and DSIR," *Journal of Electromagnetic Waves and Applications*, Vol. 24, No. 2–3, 209–218, 2010.
20. Lin, H.-J., X.-Q. Chen, X.-W. Shi, L. Chen, and C.-L. Li, "A dual passband filter using hybrid microstrip open loop resonators and coplanar waveguide slotline resonators," *Journal of Electromagnetic Waves and Applications*, Vol. 24, No. 1, 141–149, 2010.
21. Wang, J.-P., L. Wang, Y.-X. Guo, Y. X. Wang, and D.-G. Fang, "Miniaturized dual-mode bandpass filter with controllable harmonic response for dual-band applications," *Journal of Electromagnetic Waves and Applications*, Vol. 23, No. 11–12, 1525–1533, 2009.
22. Lee, J. and K. Sarabandi, "Design of triple-passband microwave filters using frequency transformations," *IEEE Trans. Microwave Theory Tech.*, Vol. 56, No. 1, 187–193, Jun. 2008.
23. Wu, H.-W. and R.-Y. Yang, "Design of a triple-passband microstrip bandpass filter with compact sizes," *Journal of Electromagnetic Waves and Applications*, Vol. 24, Nos. 17–18, 2333–2341, 2010.
24. Weng, R.-M. and P.-Y. Hsiao, "Double-layered quad-band bandpass filter for multi-band wireless systems," *Journal of Electromagnetic Waves and Applications*, Vol. 23, No. 16, 2153–2161, 2009.
25. Du, Y. and B. Liu, "A numerical method for electromagnetic scattering from dielectric rough surfaces based on the stochastic second degree method," *Progress In Electromagnetics Research*, Vol. 97, 327–342, 2009.
26. Tian, J., Z.-Q. Lv, X.-W. Shi, L. Xu, and F. Wei, "An efficient approach for multifrontal algorithm to solve non-positive-definite finite element equations in electromagnetic problems," *Progress In Electromagnetics Research*, Vol. 95, 121–133, 2009.
27. Kusiek, A. and J. Mazur, "Analysis of scattering from arbitrary configuration of cylindrical objects using hybrid finite-difference mode-matching method," *Progress In Electromagnetics Research*, Vol. 97, 105–127, 2009.
28. Ebadi, S. and K. Forooraghi, "Green's function derivation of an annular waveguide for application in method of moment analysis

of annular waveguide slot antennas," *Progress In Electromagnetics Research*, Vol. 89, 101–119, 2009.

29. Norgren, M. and B. L. G. Jonsso, "The capacitance of the circular parallel plate capacitor obtained by solving the Love integral equation using an analytic expansion of the kernel," *Progress In Electromagnetics Research*, Vol. 97, 357–372, 2009.
30. Zhang, G.-H., M. Y. Xia, and X.-M. Jiang, "Transient analysis of wire structures using time domain integral equation method with exact matrix elements," *Progress In Electromagnetics Research*, Vol. 92, 281–298, 2009.
31. Fan, Z. H., R.-S. Chen, H. Chen, and D.-Z. Ding, "Weak form nonuniform fast fourier transform method for solving volume integral equations," *Progress In Electromagnetics Research*, Vol. 89, 275–289, 2009.
32. Chang, H.-W., Y.-H. Wu, S.-M. Lu, W.-C. Cheng, and M.-H. Sheng, "Field analysis of dielectric waveguide devices based on coupled transverse-mode integral equation-numerical investigation," *Progress In Electromagnetics Research*, Vol. 97, 159–176, 2009.
33. Miraftab, V. and R. R. Mansour, "Computer-aided tuning of microwave filters using fuzzy logic," *IEEE Trans. Microwave Theory Tech.*, Vol. 50, 2781–2788, Dec. 2002.
34. Miraftab, V. and R. R. Mansour, "A robust fuzzy-logic technique for computer-aided diagnosis of microwave filters," *IEEE Trans. Microwave Theory Tech.*, Vol. 52, 450–456, Jan. 2004.
35. Tayarani, M. and Y. Kami, "Qualitative analysis in engineering electromagnetic; an application to general transmission lines," *IEIEC Transactions on Electronics*, Vol. 84, No. 3, 364–375, Mar. 2001.
36. Guney, K. and N. Sarikaya, "Resonant frequency calculation for circular microstrip antennas with a dielectric cover using adaptive network-based fuzzy inference system optimized by various algorithms," *Progress In Electromagnetics Research*, Vol. 72, 279–306, 2007.
37. Guney, K. and N. Sarikaya, "Concurrent neuro-fuzzy systems for resonant frequency computation of rectangular, circular and triangular microstrip antennas," *Progress In Electromagnetics Research*, Vol. 84, 253–277, 2008.
38. Turkmen, M., S. Kaya, C. Yildiz, and K. Guney, "Adaptive neuro-fuzzy models for conventional coplanar waveguides," *Progress In Electromagnetics Research B*, Vol. 6, 93–107, 2008.

39. Mohdeb, N. and M. R. Mekideche, "Determination of the relative magnetic permeability by using an adaptive neuro-fuzzy inference system and 2D-FEM," *Progress In Electromagnetics Research B*, Vol. 22, 237–255, 2010.
40. Ostadzadeh, S. R., M. Soleimani, and M. Tayarani, "A fuzzy model for computing input impedance of two coupled dipole antennas in the echelon form," *Progress In Electromagnetics Research*, Vol. 78, 265–283, 2008.
41. Ostadzadeh, S. R., M. Tayarani, and M. Soleimani, "A fuzzy model for computing back-scattering response from linearly loaded dipole antenna in the frequency domain," *Progress In Electromagnetics Research*, Vol. 86, 229–242, 2008.
42. Dadgarnia, A. and A. A. Heidari, "A fast systematic approach for microstrip antenna design and optimization using ANFIS and GA," *Journal of Electromagnetic Waves and Applications*, Vol. 24, No. 16, 2207–2221, 2010.
43. Kabir, H., Y. Wang, M. Yu, and Q.-J. Zhang, "High-dimensional neural-network technique and applications to microwave filter modeling," *IEEE Trans. Microwave Theory Tech.*, Vol. 58, No. 1, 145–156, Jan. 2010.
44. Takagi, T. and M. Sugeno, "Fuzzy identification of systems and its application to modeling and control," *IEEE Trans. On Systems, Man. and Cybernatics*, Vol. 15, No. 1, 116–132, Jan./Feb. 1985.
45. Takagi, T. and M. Sugeno, "A fuzzy logic approach to qualitative modeling," *IEEE Trans. On Fuzzy Systems*, Vol. 1, No. 1, 1282–1285, Feb. 1993.
46. Shouraki, S. B. and N. Honda, "Recursive fuzzy modeling based on fuzzy interpolation," *Journal of Advanced Computational Intelligence*, Vol. 3, No. 2, 114–125, Apr. 1999.
47. Shouraki, S. B. and N. Honda, "Fuzzy interpretation of human intelligence," *International Journal of Uncertainty, Fuzziness and Knowledge-based Systems*, Vol. 7, No. 4, 407–414, Aug. 1999.
48. Rizzi, P. A., *Microwave Engineering: Passive Circuits*, Prentice-Hall, 1988.